Journal of
Composites Science

MDPI

Article

Nucleation of the β-polymorph in Composites of Poly(propylene) and Graphene Nanoplatelets

Valentina Guerra, Chaoying Wan and Tony McNally *

International Institute for Nanocomposites Manufacturing (IINM), WMG, University of Warwick, Coventry CV4 7AL, UK; V.Guerra@warwick.ac.uk (V.G.); Chaoying.Wan@warwick.ac.uk (C.W.)
* Correspondence: t.mcnally@warwick.ac.uk; Tel.: +44-(0)24-7657-3256

Received: 12 March 2019; Accepted: 3 April 2019; Published: 8 April 2019

Abstract: The effects of graphene nanoplatelets (GNPs) on the nucleation of the β-polymorph of polypropylene (PP) were studied when melt-mixed at loadings of 0.1–5 wt % using a laboratory scale twin-screw (conical) extruder and a twin-screw (parallel) extruder with *L/D* = 40. At low GNP loadings (i.e., ≤0.3 wt %), the mixing efficiency of the extruder used correlated with the β-nucleating activity of GNPs for PP. GNP agglomeration at low loadings (<0.5 wt %) resulted in an increase in the β-phase fraction (K_β) of PP, as determined from X-ray diffraction measurements, up to 37% at 0.1 wt % GNPs for composites prepared using a laboratory scale twin-screw (conical) extruder. The level of GNP dispersion and distribution was better when the composites were prepared using a 16-mm twin-screw (parallel) extruder, giving a K_β increase of 24% upon addition of 0.1 wt % GNPs to PP. For GNP loadings >0.5 wt %, the level of GNP dispersion in PP did not influence the growth of β-crystals, where K_β reached a value of 24%, regardless of the type of extruder used. From differential scanning calorimetry (DSC) measurements, the addition of GNPs to PP increased the crystallization temperature (T_c) of PP by 14 °C and 10 °C for the laboratory scale extruder and 16-mm extruder, respectively, confirming the nucleation of PP by GNPs. The degree of crystallinity (X_c%) of PP increased slightly at low GNP additions (≤0.3 wt %), but then decreased with increasing GNP content.

Keywords: poly(propylene); graphene nanoplatelets (GNPs); nucleation; β-polymorph

1. Introduction

The microstructure of polymer polymorphs, in terms of crystalline content, crystallite type, and size (i.e., packing geometries) formed upon cooling, is widely influenced by processing conditions as well as the presence of additives [1]. Isotactic polypropylene (PP) (i-PP) is a polymorph thermoplastic polymer with chains arranged in a helical conformation. The polymorphism of i-PP is derived from the different crystalline geometries (unit cells) in which the helices pack, namely monoclinic (α), trigonal (β), and triclinic (γ). A metastable smectic (δ) phase consisting of helices with a highly disordered arrangement can be obtained by quenching molten i-PP below 0 °C [2,3]. The α-form is the most common and stable polymorphic phase of i-PP. However, with increasing requirements and demand for lightweight materials, there has been significant interest regarding the β-polymorph of i-PP, which has a higher impact strength and toughness than the α-polymorph of i-PP [4–6]. The mechanical properties of the β-form are associated with its peculiar broad lamellae morphology. The lamellae form coplanar stacks where the plane twists along the growth direction and the β-spherulites form exhibit 3D banded structure lamellae. A schematic of α and β crystals of PP is shown in Figure 1.

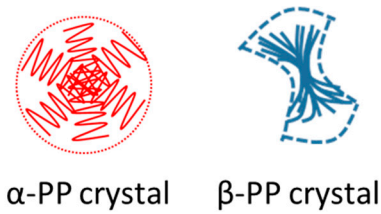

Figure 1. Schematic representation of α and β crystals of polypropylene (PP) showing a spherical and banded structure, respectively, as they would be seen under polarized light microscopy. The dotted lines contour the simulated PP chain to highlight their different arrangements in the two crystals.

As a load is applied on β-i-PP above the necking point, the banded lamellae start to separate and defold, undergoing a β- to α-phase transition. This leads to a slight increase in tensile stress (strain hardening), especially at low deformation rates. The necked specimen then deforms to break at relative high stress [7–10]. Furthermore, Jacoby et al. have reported that the coupling between the crystalline and amorphous regions in β-i-PP is weaker than in α-i-PP, thus enhancing the mechanical damping behavior of the β-form [11]. The combination of lamellae morphology, the β- to α-phase transition, and damping behavior make β-i-PP tougher than α-i-PP.

Several methodologies, including shear-induced crystallization [12–16], crystallization in a temperature field gradient, quenching from the melt, vibration-induced crystallization, ultraviolet (UV) irradiation, and the addition of specific nucleating agents have all been applied in the past years to produce β-i-PP ([10] and references therein). Previous studies have reported that the addition of 1D/2D nanomaterials to i-PP promote the nucleation and growth of β-spherulites, such as clay [17], octadecylamine-functionalized single-walled carbon nanotube (SWCNTs) [18], and graphite [19]: However, the effect of graphene nanoplatelets (GNPs) has been reported much less [3]. It has been reported that GNPs promote α-nucleating formation in PP composites prepared by twin-screw extrusion [3].

In this work, composites of i-PP and GNPs were prepared by melt mixing techniques (i.e., extrusion and injection molding) in order to study the effect of GNP addition as a β-nucleating agent for PP. We show a correlation between mixing, depending on extruder type, and the β-nucleating efficiency of GNP. As research efforts on functional composites with carbon additives continue to increase unabated for a range of diverse applications (e.g., automotive, electronics, tissue engineering) [20–23], it is essential to understand the effects of processing on the properties of the final composites. Therefore, this study aimed to correlate the effect of GNP addition on the crystallization behavior of PP and understand the role that the processing conditions employed in composite preparation play in inducing PP crystallization.

2. Materials and Methods

PP (material grade 1063L1, melt flow rate (MFR) = 8.0 g/10 min as reported in the data sheet provided by the supplier) was purchased from ExxonMobil, Baytown, TX, USA, and delivered in pellet form. GNP powder was kindly provided by Thomas Swan & Co. Ltd, Consett, UK, and had an average lateral size on the order of 10 μm and a thickness in the range of 100 nm to 200 nm.

The PP was cryo-milled to a powder in a freezer mill (SPEXSamplePrep) before being dry-mixed manually with the GNP powder. Composites of PP with GNPs up to 5 wt % were first prepared using a laboratory scale extruder (Thermo Scientific, HAAKE Lab, Waltham, MA, USA), which was fitted with twin conical screws (nonmodular, screw diameter = 5/14 mm (conical), screw length = 109.5 mm). Each composition post-melt mixing was fed directly to a microinjection molding machine (Thermo Scientific, Multijet Plus, Waltham, MA, USA) to prepare test specimens for characterization. Table 1 lists the processing conditions used to produce all samples.

Table 1. Laboratory scale microextruder and mini-injection molding processing conditions.

T (°C) Extrusion Barrel	Injection Molding *T* (°C)-Harvesting Cylinder	Injection Molding *T* (°C)-Mold Holder	Injection Pressure (bar)	Pressure after Injection (bar)	Time of Pressing (s)
175	190	50	600	200	5

The same compositions were also prepared using a 16-mm co-rotating parallel twin screw extruder (PRISM ThermoFischer Scientific), L/D = 40. The screws were fitted with feed screw (FS) 45/45 forward and mixing elements properly oriented to each other to guarantee optimal mixing conditions. In particular, the adopted screw configuration starting from the feeding zone to the die was as follows:

- 10 FS followed by 0–90°/4/12, 0°/4/12, and 90–0°/4/12 mixing elements, with respect to the last FS element offset;
- 6 FS elements followed by 0°/6/18 mixing elements;
- 9 FS elements followed by 0°/4/12, 0–90°/8/24 mixing elements;
- 7 FS elements to close the screws assembling.

The orientation of the mixing elements was based on the optimization of the highest mixing conditions (0–90°) with the lowest one (0°), as suggested by the manufacturer. The advantage of the parallel twin screw extruder over the conical one was its ability to modulate the screw configuration according to the desired properties.

The temperature profile used from the feed to the die end was set to 170 °C, 180 °C, 185 °C, 190 °C, 190 °C, 195 °C, 195 °C, 200 °C, 205 °C. The molten composite filament was drawn from the extruder, cooled in a water bath, and pelletized using a laboratory pelletizer. The pellets were collected and processed using the same microinjection molding machine and processing conditions, as per Table 1.

In both instances, disks 25 mm in diameter and 1.7 mm thick were prepared, and samples were taken from these discs for scanning electron microscopy (SEM), differential scanning calorimetry (DSC), and X-ray diffraction (XRD) measurements.

SEM imaging was carried out using a Zeiss Sigma field emission instrument, provided with a Gemini column. The images were recorded using an InLens detector, a working distance of 3.2 mm, and an acceleration voltage of 5 kV. The samples were cryo-fractured and placed on a carbon adhesive tape mounted on an aluminum SEM stub. Before testing, the samples were sputter-coated (10 nm) using a Pd/Pt metal target (Cressington 108 auto), provided with a thickness controller. The coating was applied to minimize charging on the surface of the sample due to the backscattering of the electron beam when hitting non-electrically conductive materials and under a weak argon atmosphere.

The crystalline structure of the samples was analyzed by wide-angle X-ray diffraction (WAXD), using a PANalytical Empyrean X-ray diffractometer. The instrument was equipped with a Co ($K_{\alpha 1}$ (λ) = 1.789 Å) source, a PIXcel3D detector, a tube voltage of 45 kV, and a current of 40 A. The tests were set in reflectance mode with a stage speed of 1 rps.

The thermal properties of all composites, including melting temperature (T_m), crystallization temperature (T_c), and degree of crystallinity (X_c), were measured by differential scanning calorimetry (DSC) using a Mettler Toledo DSC1. Two cycles were realized through heating from 25 °C to 200 °C at 10 °K/min and cooling to room temperature at 10 °K/min. The samples were held for 2 min at 200 °C before the cooling step and for 1 min at room temperature before the second heating cycle. The crystallinity fraction (X_c) was calculated according to the following equation:

$$X_c(\%) = \frac{\varphi_{PP} \cdot \Delta H_c}{\Delta H_{c,\infty}}, \quad (1)$$

where φ_{PP} is the mass fraction of PP in the mixture, ΔH_c is the enthalpy of crystallization during the first cooling, and $\Delta H_{c,\infty}$ is the enthalpy of crystallization of a theoretical PP crystal of infinite dimensions (207.1 J/g, [24]).

3. Results and Discussion

Figure 2 shows representative SEM images of the composite of PP with 5 wt % of GNPs prepared with a laboratory scale extruder (Figure 2a–c) and the 16-mm extruder (Figure 2d–f). The differently designed extruders imparted different levels of shear stress on the composites during melt mixing, resulting in different levels of GNP dispersion and distribution per unit volume of PP matrix. This contributed to the nucleation efficiency of GNPs for PP, particularly at low GNP loading.

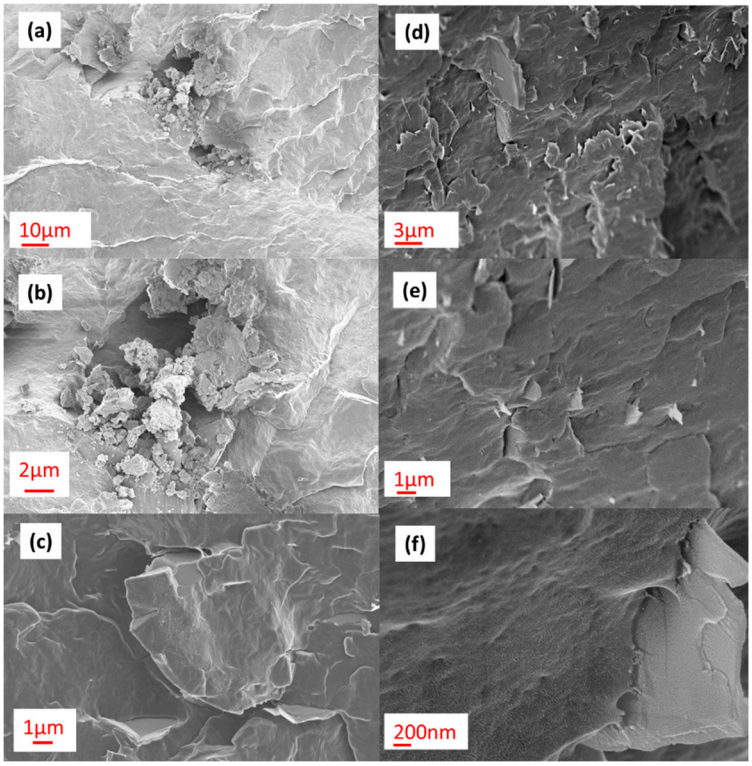

Figure 2. Scanning electron microscopy (SEM) images of a composite of PP and 5 wt % graphene nanoplatelets (GNPs) prepared by the laboratory scale extruder (**a**–**c**) and the 16-mm extruder (**d**–**f**) at different magnifications.

Irrespective of the extruder used, it became more challenging to effectively disperse the GNPs with increased loading. At 5 wt %, agglomerates of GNPs could be seen in the composite prepared by the laboratory scale extruder (Figure 2a–c). In contrast, good distribution of the GNPs in the polymer matrix was achieved when using the 16-mm extruder (Figure 2d–f) when this was examined across the length scales. The application of shear and some extensional flow in the parallel twin-screw extruder was more effective at higher GNP loadings for breaking down the GNP agglomerates during mixing in PP, with flakes of ca. 90-nm thickness observed (Figure 2f). The mixing efficiency of the two extruders influenced the crystallization behavior of PP upon addition of GNPs.

Figure 3a,b shows the XRD patterns registered for neat PP, GNPs, and their composites at different GNP loadings prepared with both extruders. The fraction of PP β-phase formed (K_β) for the composites prepared with the two different extruders as a function of GNP loading was estimated using Equation (2) [25,26]:

$$K_\beta = \frac{H_\beta}{H_\beta + H\alpha_1 + H\alpha_2 + H\alpha_3}, \quad (2)$$

where H_β is the intensity of the β(300) peak in the XRD pattern, and $H\alpha_1$, $H\alpha_2$, and $H\alpha_3$ are the intensities of the α(100), α(040), and α(130) peaks, respectively.

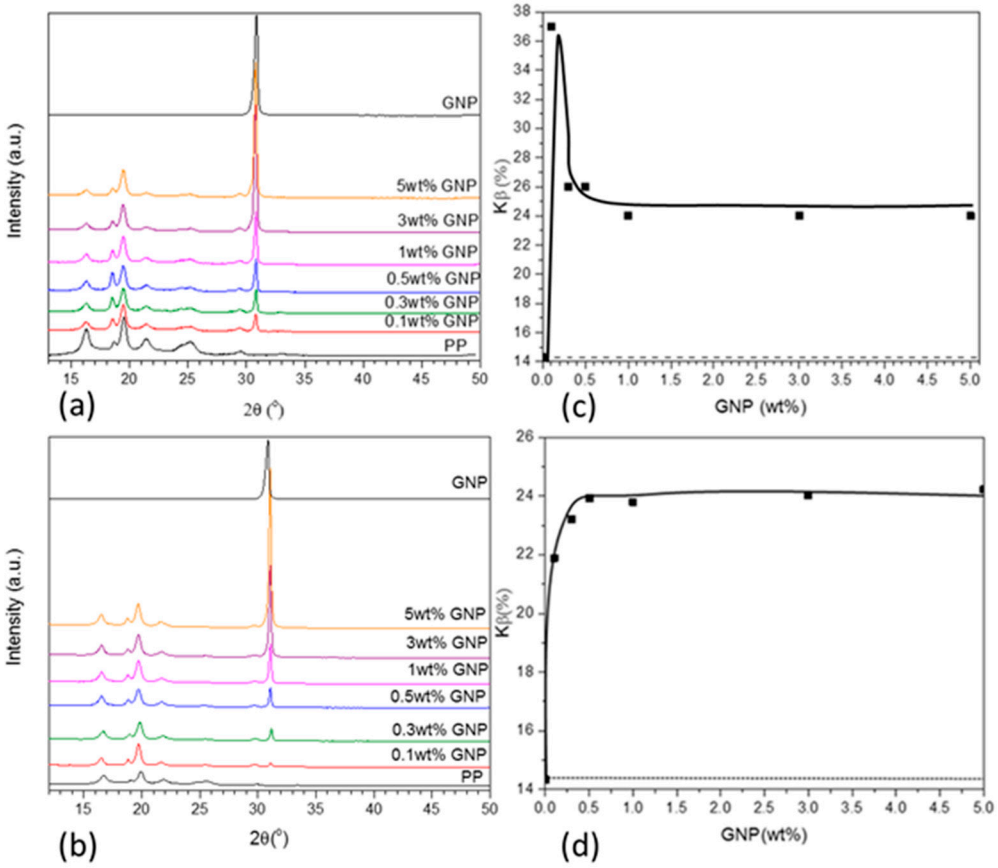

Figure 3. XRD patterns of PP, GNPs, and their composites at different GNP loadings prepared with (**a**) a laboratory scale extruder and (**b**) a 16-mm extruder, and the fraction of β-polymorph formed (K_β) as a function of GNP loading for composites prepared by (**c**) a laboratory scale extruder and (**d**) a 16-mm extruder.

The XRD patterns reported in Figure 3a,b showed the most intense peaks for PP at 2θ = 16.5° α(100), 19.2° β(300), 20° α(040), 22° α(130), and for the GNPs at 2θ = 32° (002). The registered peaks may have been shifted compared to those reported in other studies, since the X-ray source used in this work was cobalt, $K_{\alpha 1}$ (λ) = 1.789 Å [1,27]. The intensity of the single peak in the GNP pattern at 2θ = 32° due to the crystallographic plane (002) increased with increasing GNP loading, as expected. Furthermore, the peak at 2θ = 19.2° β(300) also increased with increasing GNP content, confirming the GNPs had a β-nucleating effect on this PP, irrespective of the extruder used to prepare the composites. This observation was more evident from a plot of K_β (i.e., total fraction of β-polymorph formed) as a function of GNP content in the composite. Specifically, the K_β calculated for the composites prepared by the laboratory scale extruder had a maximum of 37% at 0.1 wt % GNP, before decreasing to 24% at 0.3 wt % GNP and then remaining constant with increasing GNP loading up to 5 wt %. In contrast, the K_β calculated for the composites prepared using the 16-mm extruder increased up to 24% at GNPs = 0.5 wt % and remained constant at higher GNP loading. The difference in K_β at low GNP loading was associated with the more effective combination of GNP dispersion and particularly distribution in the 16-mm extruder. This created a system where there was greater interfacial interaction between GNP filler particles and polymers, which in turn hindered polymer chain dynamics, thus favoring the growth of β-crystallites [1]. However, the difference in K_β was evident only for GNP $\leq$0.3 wt %, since at higher GNP loadings, K_β was constant at 24%, regardless of the extruder used. Clearly, above

a critical GNP loading of 0.5 wt %, further successive additions of GNP had no further effect on β-nucleation, but it hindered polymer chain dynamics. GNP particles constrained the movement and alignment of PP chains on GNP platelets, thus limiting the formation of more β-crystals, regardless of the processing method employed. There was no further β-nucleation above 0.5 wt % GNP [1], and β-crystallite growth was more sensitive to processing at low filler concentration. It should be noted that the values for K_β may have had contributions from both processing effects and the incorporation of GNPs in PP. It has also been reported previously that injection molding can facilitate the formation of β-crystals. The melt-flow realized inside the mold upon injection creates a sample with a so-called "skin-core" morphology, where the skin is subject to high shear. That is, the skin of the sample is richer in β-spherulites, whereas the core is richer in α-spherulites [7]. In Figure 2c,d, the K_β for the neat PP is 14% (dashed line), derived from both the pre-existent β-crystals in the as-received raw material and the β-crystals formed upon injection molding. Therefore, any further increase in K_β was solely due to the β-nucleation effect upon GNP addition.

The thickness of α- and β-spherulites within neat PP and its composites at different GNP loadings was calculated using Scherrer's equation [28]:

$$L_{hkl} = \frac{k\lambda}{\beta_{hkl} cos\theta_{hkl}}, \quad (3)$$

where k is a constant depending on the modeled shape of the crystallites, with values between 0.89–0.94. In this case, a k value of 0.90 was used, as pseudospherical-shaped crystallites were considered [29,30]. Here, β_{hkl} is the FWHM (i.e. the full width at half maximum in rad) of the peak corresponding to the plane (hkl), and θ is the diffraction angle (rad) of that plane. The thickness of the spherulites was calculated along the (040) and (300) directions related to the crystalline planes α(040) and β(300), respectively. Regardless of the extruder employed, the thicknesses were estimated as 20 nm for the β-spherulites and 10 nm for the α-spherulites, in good agreement with the Transmission Electron Microscopy (TEM) evidence reported in Reference [31]. Therefore, since K_β increased with GNP loading up to 0.5 wt % GNPs and no change in the thickness of the β-lamellae was detected, it is possible to assert that GNPs facilitated the formation of either larger lamellae or a higher number of comparable/smaller lamellae than neat PP. Table 2 summarizes the main results from the XRD analysis.

Table 2. X-ray diffraction (XRD) results summary.

Material	2θ (°)	Crystalline Planes
PP	16.5	α(100)
	19.2	β(300)
	20	α(040)
	22	α(130)
	25	α(111) + β(301)
	25.7	α(041) + α(131)
	30	α(060)
GNPs	32	(002)
K_β	24% at GNP $\geq$ 0.5 wt %	
L_{hkl}	β-spherulites = 20 nm (0–5 wt % GNP) α-spherulites = 10 nm (0–5 wt % GNP)	

Figure 4 shows the DSC curves for neat PP and composites of PP with different loadings of GNPs.

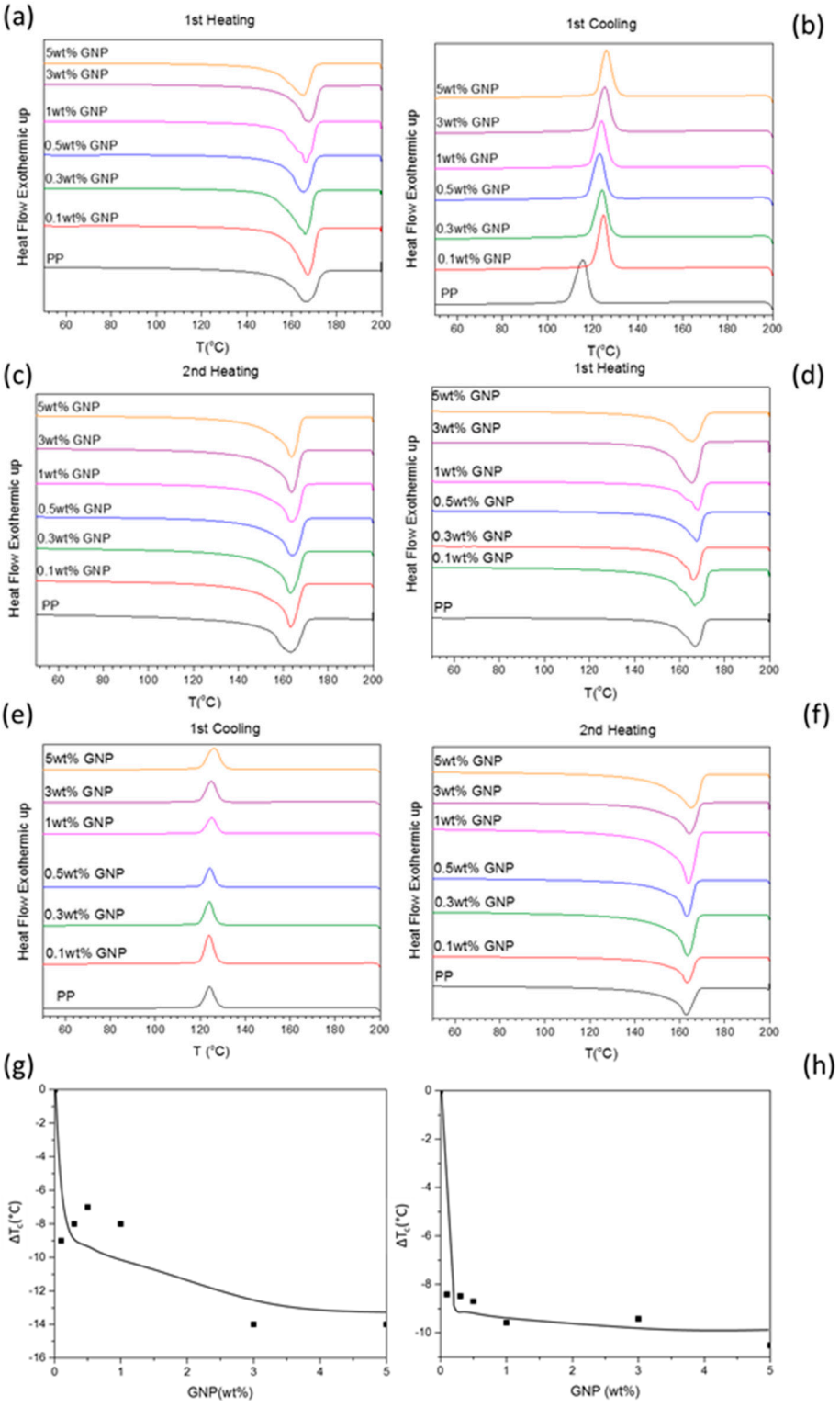

Figure 4. Differential scanning calorimetry (DSC) thermograms (heating and cooling) of composites of PP with GNPs at different loadings prepared using a laboratory scale extruder (**a**–**c**) and a 16-mm extruder (**d**–**f**) and the change in crystallization temperature (ΔT_c) as a function of GNP loading for the samples prepared with a laboratory scale extruder (**g**) and a 16-mm extruder (**h**).

The first heating thermograms (Figure 3a,d) show broad and asymmetric peaks confirming the coexistence of α-PP and β-PP crystals, as evident from the shoulder in the melting peaks at around

165.5 °C, for a GNP loading of 1 wt % for the samples prepared with the laboratory scale extruder and 0.1 wt % and 0.3 wt % for the ones prepared with the twin-screw extruder. These results suggest a change in PP polymorphism upon filler incorporation, as previously confirmed by XRD experiments. However, the β-PP polymorph content increased from the neat PP to the composites with 0.5 wt % GNPs in the XRD spectra, but a similar trend was not visible in the DSC thermograms. The reason for this discrepancy may have been due to the β–α phase transition during the first heating step in the DSC experiment, which resulted in overlapping of the peaks associated with the two polymorphic forms [3].

The first cooling thermograms (Figure 4b,e) show a shift toward higher temperatures upon GNP incorporation. In particular, T_c increased from 116 °C for the neat polymer to 132 °C and 126 °C for the composites with 5 wt % of GNPs prepared by the laboratory scale extruder and the 16-mm extruder, respectively. For composites prepared using the 16-mm extruder, the nucleation of PP upon addition of GNPs manifested as an increase in the T_c of PP, obtained for a GNP loading as low as 0.1 wt % GNP. Further increasing the loadings of GNPs did not result in more nucleation or increased T_c. This may have been associated with the even distribution of GNPs throughout the PP matrix, which constrained PP chains in a confined space delimited by filler particles, thus delaying crystallization with no further increase in T_c.

The second heating thermograms (Figure 4c,f) show broad peaks after GNP addition, yet are more symmetric than those obtained during the first heating. The controlled cooling cycle realized during the DSC measurements produced a material with a narrower crystallite size distribution compared to the material cooled by injection molding (i.e., narrower peaks should have been recorded during the second heating cycle). However, the melting peaks (T_m) of the composites in the second heating thermograms (Figure 4c,f) are as broad as the ones in the first heating curves. This was because of the β–α phase transition, which caused superimposing of the peaks related to the β–α phase transition and α-spherulite melting [10,26].

The variation in crystallization temperature (ΔT_c) recorded during the first cooling cycle (for the composites prepared with both extruders) as a function of GNP loading is reported in Figure 4g,h. A nucleating effect (ΔT_c increase) was detected for the samples prepared using both extruders: However, ΔT_c increased by up to 14 °C and 10 °C for the composites prepared using the laboratory scale and 16-mm extruder, respectively, for a GNP loading of 5 wt %. The thermal properties determined from the DSC measurements are listed in Table 3.

Table 3. Melting temperature (T_m) and enthalpy of melting (ΔH_m) from the second heating; crystallization temperature (T_c), enthalpy of crystallization (ΔH_c), and crystallinity (X_c%) from the first cooling at different GNP loadings; a/b = samples prepared by 16-mm extruder/samples prepared by laboratory scale extruder.

Filler Content (wt %)	T_m (°C) Second Heating (a/b)	ΔH_m (J/g) Second Heating (a/b)	T_c (°C) First Cooling (a/b)	ΔH_c (J/g) First Cooling (a/b)	X_c (%) First Cooling (a/b)
0	170	102	116	97	47
0.1	163/163	109/101	124/125	100/97	48/47
0.3	163/163	111/106	124/124	103/99	50/47
0.5	163/164	110/103	124/123	102/95	49/45
1	164/164	109/106	125/124	99/97	47/46
3	164/164	105/101	125/130	94/94	44/44
5	165/164	102/98	126/130	93/90	43/41

In Table 3, it should be noted that the T_m of PP after the second heating cycle decreased by 5 °C when 5 wt % GNPs were added, regardless of the extruder type employed. The addition of corrugated GNP platelets [32] may have hindered the crystallization of polymer chains, especially at higher filler loadings, and thus a larger fraction of PP amorphous phase formed and T_m was depressed. This phenomenon was evident from the change in crystalline content (X_c%), which increased to 50% when

GNPs were added at 0.5 wt % before decreasing to 43% when GNPs were added at loadings up to 5 wt % for the samples prepared by the 16-mm extruder. At GNPs $\leq$ 0.5 wt %, PP chains were free to crystallize in a defined geometry, which was more unlikely to happen at higher filler loadings >0.5 wt % due to the constraint realized by GNP particles [1]. Furthermore, GNP particles are thermally conductive (values of up to 7000 W/mK at room temperature have been reported [33,34]), whereas PP is a thermal insulator: Thus, a more efficient thermal dissipation was realized during the cooling cycle where GNP particles were present, forcing nearby neighbor PP chains to crystallize faster than those further away. This might have contributed to the formation of the amorphous phase. Crystallinity (%) did not follow any particular (allowing for DSC error) trend for the samples prepared with the laboratory scale extruder, perhaps due to variable and non-uniform distribution of GNPs in PP.

The values of T_c and the degree of crystallinity (%) for PP upon GNP addition revealed that the most effective nucleating effect occurred for a GNP loading of 0.5 wt %, which coincided with a saturation of the β-nucleating effect (detected from XRD measurements) (Figure 3). However, it was not possible to make informed conclusions on the β-nucleation of PP by GNPs from the DSC results, as the heating and cooling cycles resulted in an overlapping of the α–β transition and the α-polymorph crystallization during the first cooling, regardless of the type of extruder used [7,10]. ΔH_m and ΔH_c of the composites prepared using the 16-mm extruder increased upon addition of up to 0.5 wt % GNPs to PP (i.e., either thicker or larger lamellae formed during the heating and cooling cycles. When 5 wt % GNPs were added, ΔH_m and ΔH_c decreased, probably due to the increase in the amorphous phase. This trend was not detected for the samples prepared by the laboratory scale extruder due to the inhomogeneity of the samples obtained with this process (GNP agglomeration, see Figure 2).

4. Conclusions

GNPs readily nucleated the β-polymorph of PP regardless of the extruder type used to prepare their composites (i.e., laboratory scale twin-screw (conical) extruder and L/D = 16 twin-screw (parallel) extruder; see XRD). Furthermore, the mixing efficiency when preparing composites of PP and GNPs at low filler loadings (<0.5 wt %) influenced the formation of β-crystals within the PP matrix. For low GNP loadings (<0.5 wt %), dispersion and distribution of GNPs was optimal, PP chain mobility was more hindered, and the formation of the β-conformation was preferred. However, the mixing efficiency was less relevant at higher filler loadings (i.e., >0.5 wt %), since above this the GNP loading saturation of the β-nucleating effect was obtained. For that reason, no further increase of the β-fraction (K_β) at GNP loadings >0.5 wt % was observed, irrespective of the extruder used (i.e., low and high mixing efficiency; see SEM, XRD), with a saturation value of 24% (see XRD).

The nucleating effect of GNPs on PP was also confirmed from the DSC experiments, with an increase in T_c of ca. 14 °C and 10 °C for the samples prepared using the laboratory scale extruder and the 16-mm extruder, respectively. For the composites prepared with the latter, the 10 °C increase in the T_c of PP was obtained with just 0.1 wt % GNPs, and further successive increasing loadings of GNPs up to 5 wt % had little or no effect (allowing for instrument error) on T_c. The GNPs were more widely distributed within the PP matrix, and the polymer chains were more constrained, which delayed crystallization. The addition of GNPs at ca. 0.5 wt % increased the PP crystallinity to ca. 50% when using the 16-mm extruder, whereas no difference was detected when using the laboratory scale extruder, probably due to the high filler agglomeration in PP (see SEM). At filler loadings >0.5 wt %, the crystallinity decreased and a higher fraction of amorphous phase formed. Moreover, during cooling, there may have been a contribution to the crystallization behavior observed given the high thermal conductivity of GNPs, which contributed to more efficient heat dissipation in the immediate environment of the GNP particles, forcing nearby PP chains to crystallize faster than those further away, leading to a reduction in crystalline content.

Author Contributions: Conceptualization, T.M.; Methodology, V.G. and T.M.; Investigation, V.G.; Writing-Original Draft Preparation, V.G.; Writing-Review & Editing, V.G., C.W. and T.M.; Supervision, C.W. and T.M.; Funding Acquisition, T.M.

Funding: V.G. thanks the EPSRC (EP/L016389/1) and Thomas Swan Ltd. for funding an EngD studentship.

Conflicts of Interest: The authors declare no conflicts of interest.

References

1. Kalaitzidou, K.; Fukushima, H.; Askeland, P.; Drzal, L.T. The nucleating effect of exfoliated graphite nanoplatelets and their influence on the crystal structure and electrical conductivity of polypropylene nanocomposites. *J. Mater. Sci.* **2008**, *43*, 2895–2907. [CrossRef]
2. Saraf, R.; Porter, R.S. Considerations on the structure of smectic polypropylene. *Mol. Cryst. Liq. Cryst.* **1985**, *2*, 85–93.
3. Dai, J.; Shen, Y.; Yang, J.H.; Huang, T.; Zhang, N.; Wang, Y. Crystallization and melting behaviors of polypropylene admixed by graphene and beta-phase nucleating agent. *Colloid Polym. Sci.* **2014**, *292*, 923–933. [CrossRef]
4. Tjong, S.C.; Shen, J.S.; Li, R.K.Y. Impact fracture-toughness of beta-form polypropylene. *Scr. Metall. Mater.* **1995**, *33*, 503–508. [CrossRef]
5. KargerKocsis, J.; Varga, J.; Ehrenstein, G.W. Comparison of the fracture and failure behavior of injection-molded alpha- and beta-polypropylene in high-speed three-point bending tests. *J. Appl. Polym. Sci.* **1997**, *64*, 2057–2066. [CrossRef]
6. Varga, J.; Ehrenstein, G.W.; Schlarb, A.K. Vibration welding of alpha and beta isotactic polypropylenes: Mechanical properties and structure. *Express Polym. Lett.* **2008**, *2*, 148–156. [CrossRef]
7. Varga, J. β-modification of isotactic polypropylene: Preparation, structure, processing, properties, and application. *J. Macromol. Sci.* **2002**, *B41*, 1121–1171. [CrossRef]
8. KargerKocsis, J.; Varga, J. Effects of β-α transformation on the static and dynamic tensile behavior of isotactic polypropylene. *J. Appl. Polym. Sci.* **1996**, *62*, 291–300. [CrossRef]
9. Chen, H.B.; Karger-Kocsis, J.; Wu, J.S.; Varga, J. Fracture toughness of alpha- and beta-phase polypropylene homopolymers and random- and block-copolymers. *Polymer* **2002**, *43*, 6505–6514. [CrossRef]
10. Papageorgiou, D.G.; Chrissafis, K.; Bikiaris, D.N. β-Nucleated Polypropylene: Processing, Properties and Nanocomposites. *Polym. Rev.* **2015**, *55*, 596–629. [CrossRef]
11. Jacoby, P.; Bersted, B.H.; Kissel, W.J.; Smith, C.E. Studies on the beta-crystalline form of isotactic polypropylene. *J. Polym. Sci. B* **1986**, *24*, 461–491. [CrossRef]
12. Varga, J.; KargerKocsis, J. Rules of supermolecular structure formation in sheared isotactic polypropylene melts. *J. Polym. Sci. B* **1996**, *34*, 657–670. [CrossRef]
13. Zhang, C.G.; Hu, H.Q.; Wang, D.J.; Yan, S.; Han, C.C. In situ optical microscope study of the shear-induced crystallization of isotactic polypropylene. *Polymer* **2005**, *46*, 8157–8161. [CrossRef]
14. Nogales, A.; Hsiao, B.S.; Somani, R.H.; Srinivas, S.; Tsou, A.H.; Balta-Calleja, F.J.; Ezquerra, T.A. Shear-induced crystallization of isotactic polypropylene with different molecular weight distributions: In situ small- and wide-angle X-ray scattering studies. *Polymer* **2001**, *42*, 5247–5256. [CrossRef]
15. Somani, R.H.; Hsiao, B.S.; Nogales, A.; Srinivas, S.; Tsou, A.H.; Sics, I.; Balta-Calleja, F.J.; Ezquerra, T.A. Structure development during shear flow-induced crystallization of i-PP: In-situ small-angle X-ray scattering study. *Macromolecules* **2000**, *33*, 9385–9394. [CrossRef]
16. Moitzi, J.; Skalicky, P. Shear-induced crystallization of isotactic polypropylene melts-isothermal waxs experiments with synchrotron-radiation. *Polymer* **1993**, *34*, 3168–3172. [CrossRef]
17. KargerKocsis, J. How does "phase transformation toughening" work in semicrystalline polymers? *Polym. Eng. Sci.* **1996**, *36*, 203–210. [CrossRef]
18. Grady, B.P.; Pompeo, F.; Shambaugh, R.L.; Resasco, D.E. Nucleation of polypropylene crystallization by single-walled carbon nanotubes. *J. Phys. Chem. B* **2002**, *106*, 5852–5858. [CrossRef]
19. Gopakumar, T.G.; Page, D. Polypropylene/graphite nanocomposites by thermo-kinetic mixing. *Polym. Eng. Sci.* **2004**, *44*, 1162–1169. [CrossRef]
20. Li, B.; Zhong, W.H. Review on polymer/graphite nanoplatelet nanocomposites. *J. Mater. Sci.* **2011**, *46*, 5595–5614. [CrossRef]
21. Scaffaro, R.; Maio, A.; Lopresti, F.; Botta, L. Nanocarbons in Electrospun Polymeric Nanomats for Tissue Engineering: A Review. *Polymers* **2017**, *9*, 76. [CrossRef]

22. Scaffaro, R.; Maio, A.; Botta, L.; Gulino, E.F.; Gulli, D. Tunable release of Chlorhexidine from Polycaprolactone-based filaments containing graphene nanoplatelets. *Eur. Polym. J.* **2019**, *110*, 221–232. [CrossRef]
23. Li, Y.F.; Zhu, J.H.; Wei, S.Y.; Ryu, J.; Sun, L.Y.; Guo, Z.H. Poly(propylene)/Graphene Nanoplatelet Nanocomposites: Melt Rheological Behavior and Thermal, Electrical, and Electronic Properties. *Macromol. Chem. Phys.* **2011**, *212*, 1951–1959. [CrossRef]
24. Jose, S.; Aprem, A.S.; Francis, B.; Chandy, M.C.; Werner, P.; Alstaedt, V.; Thomas, S. Phase morphology, crystallisation behaviour and mechanical properties of isotactic polypropylene/high density polyethylene blends. *Eur. Polym. J.* **2004**, *40*, 2105–2115. [CrossRef]
25. Huo, H.; Jiang, S.C.; An, L.J.; Feng, J.C. Influence of shear on crystallization behavior of the beta phase in isotactic polypropylene with beta-nucleating agent. *Macromolecules* **2004**, *37*, 2478–2483. [CrossRef]
26. Juhasz, P.; Varga, J.; Belina, K.; Belina, G. Efficiency of beta-nucleating agents in propylene/alpha-olefin copolymers. *J. Macromol. Sci. B* **2002**, *B41*, 1173–1789. [CrossRef]
27. Yi, Q.F.; Wen, X.F.; Dong, J.Y.; Han, C.C. A novel effective way of comprising a beta-nucleating agent in isotactic polypropylene (i-PP): Polymerized dispersion and polymer characterization. *Polymer* **2008**, *49*, 5053–5063. [CrossRef]
28. Guerra V, V.; Wan, C.; Sloan, J.; Degirmenci, V.; Presvytis, D.; McNally, T. 2D Boron Nitride Nanosheets (BNNS) Prepared by High-Pressure-Homogenisation: Structure and Morphology. *Nanoscale* **2018**, *10*, 19469–19477. [CrossRef]
29. Nazarov, A.S.; Demin, V.N.; Grayfer, E.D.; Bulavchenko, A.I.; Arymbaeva, A.T.; Shin, H.J.; Choi, J.Y.; Fedorov, V.E. Functionalization and dispersion of hexagonal boron nitride (h-BN) nanosheets treated with inorganic reagents. *Chem. Asian J.* **2012**, *7*, 554–560. [CrossRef]
30. Langford, J.I.; Wilson, A.J.C. Seherrer after Sixty Years: A Survey and Some New Results in the Determination of Crystallite Size. *J. Appl. Cryst.* **1978**, *11*, 102–113. [CrossRef]
31. Li, J.X.; Cheung, W.L. On the deformation mechanisms of beta-polypropylene: 1. Effect of necking on β-phase PP crystals. *Polymer* **1998**, *39*, 6935–6940. [CrossRef]
32. Preobrajenski, A.B.; Ng, M.L.; Vinogradov, A.S.; Martensson, N. Controlling graphene corrugation on lattice-mismatched substrates. *Phys. Rev. B* **2008**, *78*, 073401. [CrossRef]
33. Pop, E.; Varshney, V.; Roy, A.K. Thermal properties of graphene: Fundamentals and applications. *MRS Bull.* **2012**, *37*, 1273–1281. [CrossRef]
34. Kim, H.S.; Bae, H.S.; Yu, J.; Kim, S.Y. Thermal conductivity of polymer composites with the geometrical characteristics of graphene nanoplatelets. *Sci. Rep.* **2016**, *6*, 26825. [CrossRef]